Computers and Geotechnics 69 (2015) 46–57

Contents lists available at ScienceDirect

Computers and Geotechnics

journal homepage: www.elsevier.com/locate/compgeo

Research Paper

Modelling creep behaviour of anisotropic soft soils

Nallathamby Sivasithamparam [a,*], Minna Karstunen [b,c], Paul Bonnier [d]

[a] Computational Geomechanics Division, Norwegian Geotechnical Institute, Oslo, Norway
[b] Chalmers University of Technology, Gothenburg, Sweden
[c] Department of Civil Engineering, University of Strathclyde, Glasgow, UK
[d] PLAXIS B.V, Delft, The Netherlands

ARTICLE INFO

Article history:
Received 4 November 2014
Received in revised form 11 March 2015
Accepted 18 April 2015

Keywords:
Constitutive model
Creep
Time dependence
Anisotropy
Clays
Numerical modelling
Embankment

ABSTRACT

This paper presents a three dimensional constitutive model that describes the creep behaviour of natural clays with anisotropic stress–strain response, focussing on robust model implementation. Creep is formulated using the concept of a constant rate of visco-plastic multiplier, resulting in a formulation with easily determined creep parameters. A key assumption in the model formulation is that there is no purely elastic domain. Of the 10 input parameters that can be defined based on standard laboratory testing, five are similar to those used in the Modified Cam-Clay model. The performance of the model at element level and boundary value level is demonstrated, for the latter by comparing the simulations with the measured response of Murro test embankment in Finland. For comparison, the simulations are also done using the previously published anisotropic creep model and an equivalent rate-independent model. This enables studying the role of evolution anisotropy and creep at boundary value level by systematic comparisons.

1. Introduction

In recent years, various constitutive models have been proposed to describe fundamental features of natural soil behaviour, such as anisotropy, structure and rate-dependence (e.g. [1–5]). Different approaches have been used to capture the various rate-dependent phenomena, such as strain-rate effects, creep, relaxation and accumulated effects. These constitutive models include empirical models, rheological models and general stress–strain–time models that are based on theories of visco-plasticity. Visco-plastic models are easily adaptable to numerical implementation in a general purpose finite element framework, as they are often formulated in incremental form.

Most of the rate-dependent models were developed based on the Perzyna's [6,7] overstress theory (e.g. [1,2,4,8]). This approach has become a preferred basis for the further development of viscoplastic models. However, determination of model input parameters for overstress models is difficult (see e.g. [4]), and strictly speaking not feasible in practical context due to the very low loading rates required in the laboratory tests. As a consequence, the input values require calibration via parametric studies, which limits its practical adaptation, and furthermore, the values for the input parameters are not necessarily unique. The latter can lead to unrealistic predictions in some stress paths when applied in 3D stress space. As discussed by Yin et al. [5], the major assumption in the classic overstress models – that viscoplastic strain will not occur inside the static yield surface (i.e. there is a purely elastic region) – is in conflict with the experimental observations. It is commonly thought that a consequence of the overstress theory is that it lacks the capability to model tertiary creep, i.e. the acceleration of the creep process [9], but as shown by Yin et al. [5] this problem can be overcome by introducing some damage or destructuration law in the formulation. However, it is only possible to model stress relaxation if the stress state lies outside the current static yield surface.

As an alternative, the concept of Nonstationary Flow Surface (NSFS) theory has been used to model visco-plastic behaviour of soils in general stress space (e.g. [10,11]). According to Liingaard et al. [12] this approach has the following limitations:

(1) NSFS theory cannot describe the relaxation process when it is initiated from a stress state inside the yield surface (flow surface).
(2) The creep process initiated from a stress state inside the yield surface cannot be predicted satisfactorily.

* Corresponding author at: Computational Geomechanics Division, Offshore Energy, Norwegian Geotechnical Institute (NGI), PO Box 3930, Ullevål Stadion, No-0806 Oslo, Norway. Tel.: +47 406 94 933; fax: +47 22 23 04 48.
E-mail addresses: nallathamby.siva@ngi.no (N. Sivasithamparam), minna.karstunen@chalmers.se (M. Karstunen), p.bonnier@plaxis.nl (P. Bonnier).

http://dx.doi.org/10.1016/j.compgeo.2015.04.015
0266-352X/

Notation

α_0	initial value of anisotropy
α	scalar value of anisotropy
$\boldsymbol{\alpha}_d$	deviatoric fabric tensor
β	creep exponent
$\boldsymbol{\delta}_{ij}$	Kronecker's delta
ε_a	axial strain
ε_r	radial strain
ε_v	volumetric strain
ε_q	deviatoric strain
$\dot{\varepsilon}$	strain rate
$\dot{\varepsilon}^e$	elastic strain rate
$\dot{\varepsilon}^c$	creep strain rate
$\dot{\varepsilon}^e_v$	volumetric elastic strain rate
$\dot{\varepsilon}^e_q$	deviatoric elastic strain rate
$d\boldsymbol{\varepsilon}_d$	incremental deviatoric strain tensor
$\dot{\boldsymbol{\varepsilon}}^c_{ij}$	creep strain rate tensor
σ'_a	effective axial strain
σ'_r	effective radial strain
$\boldsymbol{\sigma}'_d$	deviatoric stress tensor
κ^*	modified swelling index
λ^*	modified compression index
λ	slope of normal compression line
η	stress ratio
η_0	stress ratio corresponding K_0 state
μ^*	modified creep index
υ'	Poisson's ratio
τ	reference time
θ_α	lode angle
ω	rate of rotation
ω_d	rate of rotation due to deviator stress
C_α	creep index
CSS	current stress surface
$\boldsymbol{D}_{ijhk}$	stiffness matrix
e_0	initial void ratio
G	shear modulus
$\boldsymbol{I}$	identity matrix
$(J_2)_\alpha$	modified second invariant to α-line
$(J_3)_\alpha$	modified third invariant to α-line
K	elastic bulk modulus
K_0^{nc}	lateral earth pressure at rest for normally consolidated state
$M(\theta)$	stress ratio at critical state
M_c	stress ratio at critical state in triaxial compression
M_e	stress ratio at critical state in triaxial extension
NCS	normal consolidation surface
OCR	over-consolidation ratio
p'	mean effective stress
p'_p	effective preconsolidation pressure
p'_{p0}	initial effective preconsolidation pressure
p'_{eq}	effective equivalent mean stress
POP	pre-overburden pressure
q	deviatoric stress
Δt	time increment

Yet another approach is to develop more general rate-dependent constitutive laws based on one dimensional empirical formulations, such as the model by Yin et al. [13] Yin and Graham [14], which has subsequently been extended to 3D e.g. by Yin et al. [15] and Yin et al. [16], and further modified e.g. by Bodas Freitas et al. [17]. However, these models contain concepts, which are perhaps difficult to understand, such as equivalent time or time shift, and the models mentioned ignore some key features of natural soil behaviour, such as anisotropy. One of the most used models in the category of empirical models is the isotropic Soft Soil Creep model [18,19] available in the commercial Plaxis finite element suite. Further developments of that model, based on the ideas of Bjerrum and Janbu, have been proposed by several authors (e.g. [3,20]).

Natural clays generally exhibit both elastic and plastic anisotropic behaviour as result of sedimentation and consolidation. For normally and slightly overconsolidated clays, anisotropic behaviour due to elastic strains can be neglected in most loading problems, as the magnitudes of elastic strains in natural soft clays are insignificant compared to plastic strains. This assumption makes a constitutive model simpler in terms of modelling and parameter determination. The anisotropic creep model (ACM) proposed by Leoni et al. [3] accounts for the initial anisotropy and the evolution of anisotropy in a simple manner, as an anisotropic extension of the isotropic Soft Soil Creep model. ACM uses rotated ellipses (similar to the S-CLAY1 model by Wheeler et al. [21]) as contours of volumetric creep strain rates. This approach overcomes the following limitations of the overstress theory:

1. Determination of viscous parameters is straight forward: ACM uses a modified creep index μ^* as input parameter for soil viscosity, which can be derived from the secondary compression coefficient C_α. This value can be easily obtained from laboratory tests and is internationally known, in contrast to the time-resistance concept adopted by Grimstad et al. [20].
2. The reference time τ has a clear link to the type of tests used in defining the apparent preconsolidation pressure (see [3] for details). Same value of τ can be adopted for modelling element test and a boundary value problem on the same soil as the test.
3. The model assumes that there is no purely elastic domain in contrast to the classic overstress theory, allowing for creep within the Normal Consolidation Surface.

However, as discussed by Sivasithamparam et al. [22] and Karstunen et al. [23], the consequences of adopting the concept of contours of constant volumetric creep strain rate are severe, as illustrated later on:

1. The ACM model cannot predict swelling on the 'dry' side of the critical state line, as it does not allow the stress state to cross the failure line represented by the Mohr–Coulomb criterion. Because of this, the ACM is limited to the 'wet' side of the critical state line only.
2. The ACM model cannot reach the critical state condition with shearing at constant volume and effective stresses, given the volumetric creep rates are assumed to be constant throughout the stress space. In its finite element implementation, the critical state condition is artificially imposed by switching to Mohr Coulomb failure criterion with zero dilatancy when approaching failure, resulting in a "jump" in the predicted stress–strain curve.
3. The ACM model cannot reproduce the isotach behaviour observed in natural soft clays under a stepwise change in strain-rate in undrained triaxial tests and CRS tests.

4. The stress paths simulated by ACM cannot overpass the critical state for normally consolidated clay, which is not in agreement with experimental observations on slightly structured or reconstituted clays [24].

The Creep-SCLAY1 model, presented in this paper, can be considered as a special kind of extended over-stress model similarly to, e.g., the Yin et al. [5] model. In contrast to the latter, the model is initially derived from an empirical equation similarly to ACM. The formulation of the Creep-SCLAY1 model makes it a special kind of extended over-stress model in the sense that:

(1) The rate of the plastic multiplier is derived based on an empirical equation rather than a consistency rule.
(2) The stress state is allowed to be outside the Normal Consolidation Surface, because no consistency rule is applied.

The first part of this paper gives a description of the Creep-SCLAY1 model and discusses briefly the ease of determination of the input parameters. Subsequently, a robust numerical implementation compatible with most general finite element codes and Plaxis in particular as a user-defined soil model is discussed. The latter two features (i.e. ease of parameter determination and robust implementation within a framework of commercial FE code) make the model ideal for the use of practising engineers, as well as researchers who do not want to implement their own models, but yet require an advanced creep model for understanding their data. The model will be useful for e.g. planning test programmes for accounting for viscous effects of soft clays and peats, as well as studying installation effects of pile and ground improvement the field. The performance of the model is then demonstrated by numerical simulations that are validated against the data from Murro test embankment, studying the effect of evolution of anisotropy and creep on the results.

2. Constitutive model Creep-SCLAY1

For the sake of simplicity, the mathematical formulation of the model in the following is presented in triaxial stress space, which can be used only to model the response of cross-anisotropic samples (cut vertically from the soil deposit) subject to oedometric or triaxial loading. The extension to more general stress space will then be summarised, with full details in the Appendix. For the simple case above, the stress quantities of mean effective stress $p' = (\sigma'_a + 2\sigma'_r)/3$ and deviator stress $q = (\sigma'_a - \sigma'_r)$ and strain quantities of volumetric strain $\varepsilon_v = (\varepsilon_a + 2\varepsilon_r)$ and deviator strain $\varepsilon_q = 2(\varepsilon_a - \varepsilon_r)/3$ are used, where subscripts a and r denote the axial and the radial directions, respectively, in the triaxial stress space.

The elastic and creep parts of the strain in the model are combined with an additive law, expressing the total strain rate as combination of elastic and creep components analogously to the classical elasto-plasticity theory.

$$\left.\begin{aligned}\dot{\varepsilon}_v &= \dot{\varepsilon}^e_v + \dot{\varepsilon}^c_v \\ \dot{\varepsilon}_q &= \dot{\varepsilon}^e_q + \dot{\varepsilon}^c_q\end{aligned}\right\} \tag{1}$$

where ε is strain, a dot over a symbol implies rate (differentiation with respect to time) and superscripts e and c refer to the elastic and creep components, and subscripts v and q refer volumetric and deviatoric components respectively.

A key assumption of the model is that there is no purely elastic domain, similar to ACM [3]. The isotropic and deviatoric elastic part of the model are defined simply as

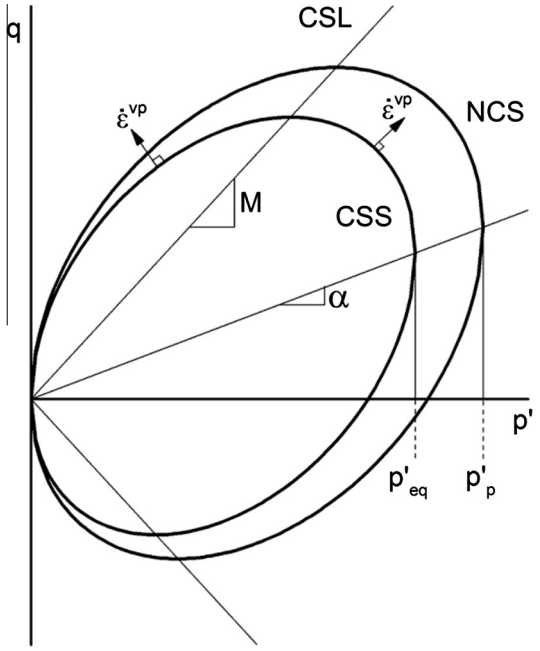

Fig. 1. Current State Surface (CSS) and Normal Consolidation Surface (NCS) of the Creep-SCLAY1 model and the direction of viscoplastic strains (triaxial stress space).

$$\dot{\varepsilon}^e_v = \frac{\dot{p}'}{k} \tag{2}$$

$$\dot{\varepsilon}^e_q = \frac{\dot{q}}{3G} \tag{3}$$

where the elastic bulk modulus $K = p'/\kappa^*$ and elastic shear modulus $G = 3p'/2\kappa^*(1-2\upsilon'/1+\upsilon')$ are stress-dependent and υ' is Poisson's ratio.

The outer rotated ellipse (see Fig. 1) defines the Normal Consolidation Surface (NCS), i.e. the boundary between small and large creep strains, and the size of this ellipse evolves with volumetric creep strains according to the hardening law

$$p'_p = p'_{p0} exp\left(\frac{\varepsilon^c_v}{\lambda^* - \kappa^*}\right) \tag{4}$$

where λ^* and κ^* are the modified compression index and modified swelling index, respectively. These are determined as the slopes of normal compression and swelling lines in volumetric strain ε_v versus $ln\ p'$ plane. The intersection of the vertical tangent to the ellipse with the p' axis is the isotropic preconsolidation pressure p'_{p0}. The inner ellipse that represents the current state of effective stress is called the Current Stress Surface (CSS). The intersection of CSS with the horizontal axis is called the equivalent mean stress p'_{eq}, and it is defined as

$$p'_{eq} = p' + \frac{(q - \alpha p')^2}{\left(M^2(\theta) - \alpha^2\right)p'} \tag{5}$$

where $M(\theta)$ is the stress ratio at critical state (dependent on Lode angle θ) and α is a scalar quantity used to describe the orientation of the normal consolidation surface and current stress surface.

Creep is formulated using the concept of a constant rate of visco-plastic multiplier, following the idea of Grimstad et al. [20] as follows

$$\dot{\Lambda} = \frac{\mu^*}{\tau}\left(\frac{p'_{eq}}{p'_p}\right)^{\beta}\left(\frac{\left(M^2(\theta) - \alpha^2_{K^{nc}_0}\right)}{\left(M^2(\theta) - \eta^2_{K^{nc}_0}\right)}\right) \tag{6}$$

where $\eta^2_{K_0^{nc}} = 3(1-K_0^{nc})/(1+2K_0^{nc})$ and the additional term $\left(M^2(\theta)-\alpha^2_{K_0^{nc}}\right)/\left(M^2(\theta)-\eta^2_{K_0^{nc}}\right)$ is added to ensure that under oedometer conditions, the resulting creep strain corresponds to the measured volumetric creep strain rate. $\alpha_{K_0^{nc}}$ defines the inclinations of the ellipses in normally consolidated state (assuming K_0 history) and μ^* is the modified creep index. To account for the rate dependency of the apparent preconsolidation pressure that is used to define the size of NCS, τ is called the reference time and is set to 1 day, if the NCS is derived from a standard 24 h oedometer test (see Leoni et al. [3] for details). The same value of τ is adopted when modelling a boundary values problem using the OCR value (overconsolidation ratio) from a standard 24 h step oedometer test and β is defined as

$$\beta = \frac{\lambda^* - \kappa^*}{\mu^*} \tag{7}$$

μ^* is related to the one-dimensional secondary compression index C_α and defined as:

$$\mu^* = \frac{C_\alpha}{\ln 10(1+e_0)} \tag{8}$$

In addition to the volumetric hardening law, the Creep-SCLAY1 model incorporates a rotational hardening law that describes the changes in the orientation of the normal consolidation surface with creep straining. This enables modelling the evolution of anisotropy due to irrecoverable strains. In triaxial stress space, the hardening law takes the following form

$$d\alpha = \omega\left(\left[\frac{3\eta}{4}-\alpha\right]\langle d\varepsilon_v^c\rangle + \omega_d\left[\frac{\eta}{3}-\alpha\right]|d\varepsilon_d^c|\right) \tag{9}$$

where $d\varepsilon_d^c$ is the increment of creep deviatoric strain, and ω and ω_d are two additional soil constants. The soil constant ω_d controls the relative effectiveness of creep shear strains and creep volumetric strains in setting the overall instantaneous target value for α (which will lie between $\frac{3\eta}{4}$ and $\frac{\eta}{3}$), whereas the soil constant ω controls the absolute rate of rotation of the yield surface towards its current target value of α. $\langle\cdot\rangle$ are Macaulay brackets. Hence, $\langle d\varepsilon_v^c\rangle = d\varepsilon_v^c$ for $d\varepsilon_v^c > 0$ and $\langle d\varepsilon_v^c\rangle = 0$ for $d\varepsilon_v^c < 0$. $|d\varepsilon_d^c|$ is a norm (absolute value) of deviatoric plastic strain.

The Creep-SCLAY1 model assumes an associated flow-rule as this is a reasonable approximation for natural clays when combined with the particular form of inclined "yield" surface [21,25] and the particular rotational hardening law in Eq. (9). Thus, the creep strain rates are calculated as

$$\dot{\epsilon}_v = \dot{\Lambda}\frac{\partial p'_{eq}}{\partial p'} \quad \text{and} \quad \dot{\epsilon}_q = \dot{\Lambda}\frac{\partial p'_{eq}}{\partial q} \tag{10}$$

In Creep-SCLAY1 model, the stress ratio at critical state (M) has been made a function of Lode angle θ. This formulation incorporates a smooth critical state surface similar to the Matsuoka and Nakai [26] failure surface, as an alternative to the Drucker–Prager failure criterion of the MCC model (see Fig. 2). Following Sheng et al. [27], the variation of $M(\theta)$ for Creep-SCLAY1 is expressed as a function of modified Lode angle given as

$$M(\theta) = M_c\left(\frac{2m^4}{1+m^4+(1-m^4)sin3\theta_\alpha}\right)^{\frac{1}{4}} \tag{11}$$

where m is defined as

$$m = \frac{M_e}{M_c} \tag{12}$$

where M_c is the value of M in triaxial compression with $\theta_\alpha = -30^\circ$, and M_e is the value of M in triaxial extension with $\theta_\alpha = 30^\circ$. A

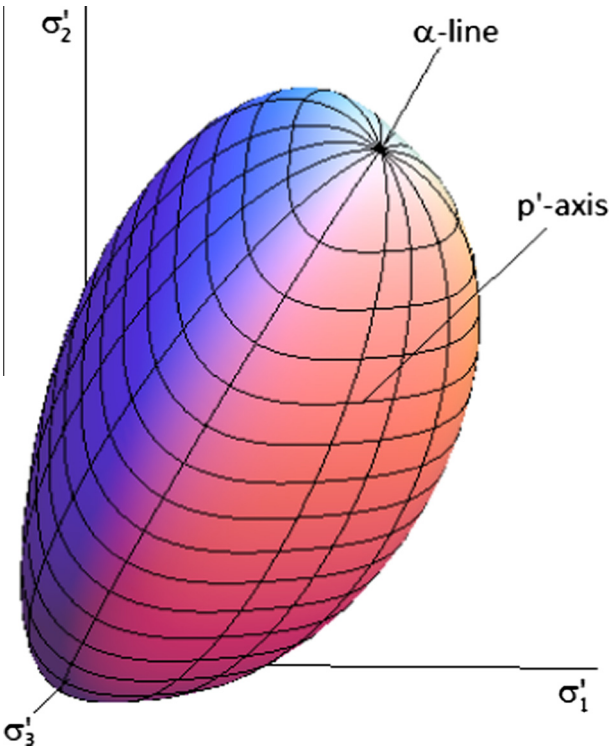

Fig. 2. The Creep-SCLAY1 model in general stress space.

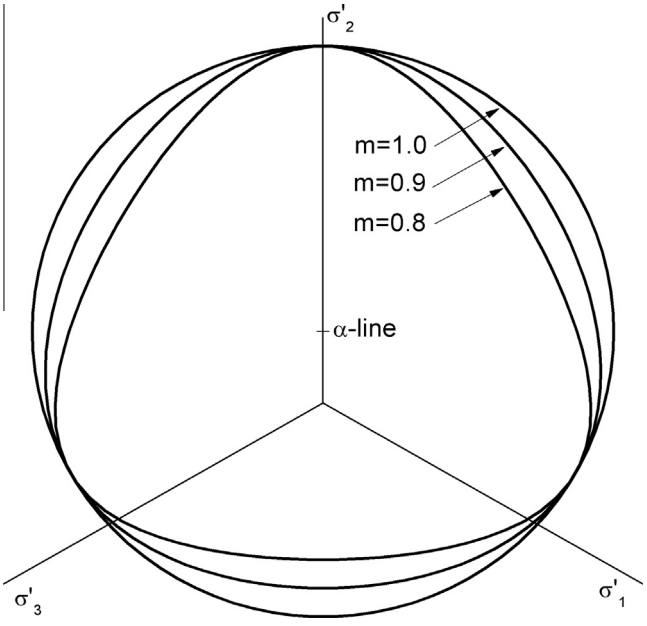

Fig. 3. Failure surface on deviatoric plane for various m values.

function of the modified Lode angle θ_α which corresponds to the stress state to the α-line and can be defined as

$$sin3\theta_\alpha = -\left[\frac{3\sqrt{3}}{2}\frac{(J_3)_\alpha}{(J_2)_\alpha^{\frac{3}{2}}}\right] \tag{13}$$

where $(J_2)_\alpha$ and $(J_3)_\alpha$ are the second and third invariants of the modified stress deviator $q-\alpha p'$, which compares the stress state with the α-line.

When M_c and M_e are equal, the failure surface reverts to the Drucker–Prager failure surface in π -plane, as shown in Fig. 3. This formulation allows a freedom in determining the failure surface between the Drucker–Prager and the Matsuoka and Nakai type failure surface, dependant on experimental evidence available. Naturally, if only *Mc* is known, input for *Me* could be calculated based on Mohr Coulomb model.

The fully generalised version of the Creep-SCLAY1 model has been included in Appendix A.

3. Parameter determination

The Creep-SCLAY1 model requires a number of soil constants and state variables as input. They can be categorised into following three groups:

1. Isotropic parameters which are similar to the Modified Cam-Clay (MCC) model [28].
2. Anisotropic parameters which are similar to the S-CLAY1 model [21].
3. Viscosity parameters which are similar to the Soft Soil Creep (SSC) model [18], and therefore the Anisotropic Creep model (ACM) [3].

Parameters which are similar to the Modified Cam-Clay model include soil constants ν' (Poisson's ratio), M (stress ratio at critical state), λ^* (modified compression index) and κ^* (modified swelling index). Strictly speaking the latter is not a constant for sensitive natural clays, but for modelling purposes the highest gradient resulting from an oedometer test can be adopted. Furthermore, the initial value for a state variable p'_p (initial size of the ellipse) is required. In the context of finite element analyses, the initial value of p'_p is calculated based on the *OCR* (vertical overconsolidation ratio) or *POP* (vertical pre-overburden pressure) and the normally consolidated K_0^{NC} value (estimated by Jaky's formula) and the anisotropy corresponding to K_0 conditions.

Parameters describing initial anisotropy (α_0) and its evolution include soil constants ω (rate of rotation of the surfaces) and ω_d (relative rate of surface rotation). The scalar value α_{K0} and ω_d can be theoretically derived based on M_c values (see Wheeler et al., [21] for details) for a soil which has had a one-dimensional consolidation history, as follows

$$\alpha_{K0} = \frac{\eta_{K0}^2 + 3\eta_{K0} - M_c^2}{3} \tag{14}$$

$$\omega_d = \frac{3}{8}\frac{4M_c^2 - 4\eta_{K0}^2 - 3\eta_{K0}}{\eta_{K0}^2 - M_c^2 + 2\eta_{K0}} \tag{15}$$

where $\eta_{K0} = 3\left(1 - K_0^{NC}\right)/1 + 2K_0^{NC}$.

By using the definition above, the model is able to have a very good K_0^{NC} prediction, in contrast to the MCC model.

The parameter ω can be estimated based on initial anisotropy α_0, modified compression index $(\lambda^*), M$ and ω_d (see Leoni et al. [3] for details) as follows

$$\omega = \frac{1}{\lambda^*} ln \frac{10MM_c^2 - 2\alpha_0\omega_d}{M_c^2 - 2\alpha_0\omega_d} \tag{16}$$

Table 1
Model parameter values for the Bothkennar clay.

λ^*	ν'	k*	M	α_0	ω	ω_d	μ^*	τ day
0.1	0.2	0.0067	1.5	0.59	50	1.0	5.07E−03	1

In derivation of the above equation, a number of major assumptions have been made (see [3]). Consequently, with certain parameter combinations the above equation might result in a negative value, which makes no physical sense. As an alternative, the empirical formula suggested by Zentar et al. [29] to estimate the ω value can be used

$$\frac{10}{\lambda^*} \leqslant \omega \leqslant \frac{20}{\lambda^*} \tag{17}$$

The values for parameter ω could be optimised by simulating an undrained triaxial extension test, if such results are available. Alternatively, if the problem is such that no significant changes in the anisotropy are expected, ω could be set to zero, hence by explicitly assuming that an initial anisotropy is fixed.

The input values for μ^* (modified creep index) can be obtained from oedometer results by plotting the volumetric strain against the logarithm of time. As shown by e.g. Karstunen and Yin [4], for natural medium sensitivity clays the value depends on stress level, because it also indirectly depends on the apparent compressibility which is varying due to the gradual process of destructuration. Hence, the input value would need to correspond to the "intrinsic value" which is reached at high stress levels. The reference time τ is linked to the definition of vertical preconsolidation stress used in the analyses, and if that is based on 24 h oedometer test, it can be set equal to one day (see Leoni et al., [3] for details) both at element and boundary value level.

4. Numerical implementation

The Creep-SCLAY1 model is implemented into the finite element code PLAXIS as a user-defined soil model (UDSM) using a fully implicit integration scheme with automatic substepping.

An integration scheme for general viscoplastic models can be found in de Borst and Heeres [30]. Strain residuals are defined over a time step Δt as

$$\begin{aligned} \boldsymbol{r}_\varepsilon &= \Delta\boldsymbol{\varepsilon}^{trial} - \left(\Delta\boldsymbol{\varepsilon}^e_{n+1} + \Delta\boldsymbol{\varepsilon}^c_{n+1}\right) \\ &= \Delta\boldsymbol{\varepsilon}^{trial} - \Delta\boldsymbol{\varepsilon}^e_{n+1} - \Delta t\dot{\Lambda}_{n+1}\left\{\frac{\partial p'_{eq}}{\partial\boldsymbol{\sigma}'}\right\}_{n+1} \end{aligned} \tag{18}$$

where Δ is increment and $\boldsymbol{r}_\varepsilon$ is strain residual vector.

Residual related to visco-plastic multiplier is defined as

$$r_\Lambda = (\Lambda_{\boldsymbol{n+1}} - \Lambda_{\boldsymbol{n}}) - \Delta t\dot{\Lambda}_{n+1} \tag{19}$$

where the subscripts n and $n+1$ denote the solutions at times t and $t+\Delta t$, respectively.

This numerical scheme always satisfies the following conditions, as the model does not have any pure elastic region

$$\Delta\boldsymbol{\varepsilon}^{trial} - \Delta\boldsymbol{\varepsilon}^e_{n+1} - \Delta t\dot{\Lambda}_{n+1}\left\{\frac{\partial p'_{eq}}{\partial\boldsymbol{\sigma}'}\right\}_{n+1} = 0 \tag{20}$$

$$(\Lambda_{\boldsymbol{n+1}} - \Lambda_{\boldsymbol{n}}) - \Delta t\dot{\Lambda}_{n+1} = 0 \tag{21}$$

The 6 strain components can be written for the iteration procedure using Taylor expansion as follows

$$\begin{aligned} &\Delta\boldsymbol{\varepsilon}^{trial} - \left(\Delta\boldsymbol{\varepsilon}^e_n + \delta\Delta\boldsymbol{\varepsilon}^e_{n+1}\right) - \left(\Delta t\dot{\Lambda}_n + \Delta t\delta\dot{\Lambda}_{n+1}\right)\left(\left\{\frac{\partial p'_{eq}}{\partial\boldsymbol{\sigma}'}\right\}_n\right. \\ &\left. + \left\{\frac{\partial p'_{eq}}{\partial^2\boldsymbol{\sigma}'^2}\right\}_{n+1}\partial\boldsymbol{\sigma}'_{\boldsymbol{n+1}}\right) = 0 \end{aligned} \tag{22}$$

By neglecting the higher order terms, and restructuring the above system of equations, the following system of equations for Newton–Raphson iterative process can be derived

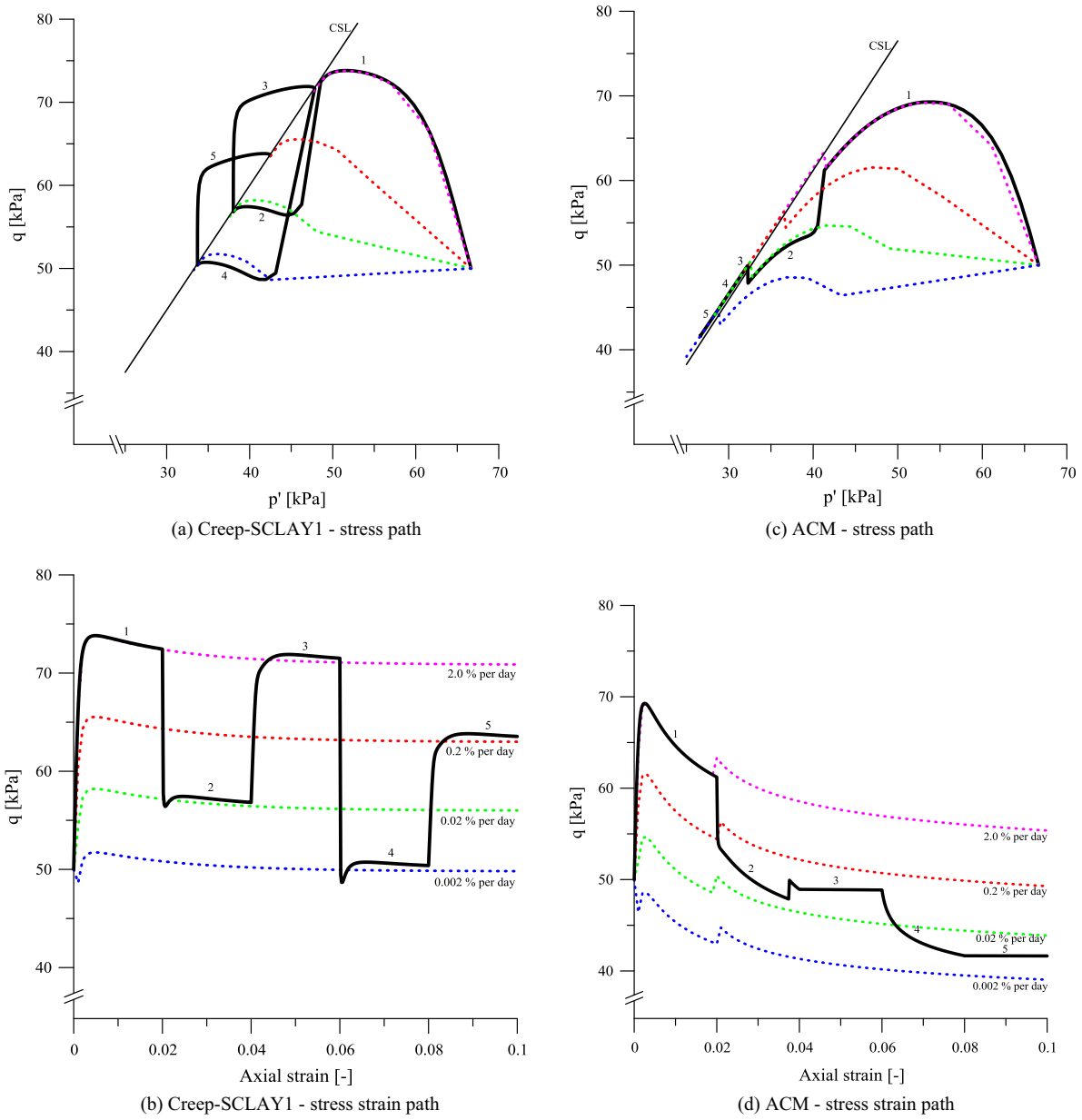

(a) Creep-SCLAY1 - stress path

(c) ACM - stress path

(b) Creep-SCLAY1 - stress strain path

(d) ACM - stress strain path

Fig. 4. Simulations of undrained triaxial compression with varying strain rate.

$$\left(\mathbf{I}+\Delta t\dot{\Lambda}_n\left\{\frac{\partial^2 p'_{eq}}{\partial\boldsymbol{\sigma}'^2}\right\}_{n+1}\boldsymbol{D}_{n+1}\right)\delta\Delta\boldsymbol{\varepsilon}^e_{n+1}+\left\{\frac{\partial p'_{eq}}{\partial\boldsymbol{\sigma}'}\right\}_n\Delta t\delta\dot{\Lambda}_{n+1}$$
$$=\Delta\boldsymbol{\varepsilon}^{trial}-\Delta\boldsymbol{\varepsilon}^e_n-\Delta t\dot{\Lambda}_n\left\{\frac{\partial p'_{eq}}{\partial\boldsymbol{\sigma}'}\right\}_n \tag{23}$$

where $\boldsymbol{D}$ is the mean stress dependent isotropic elasticity matrix.

The plastic multiplier residual can be expanded using Taylor expansion (higher order terms are again neglected) as

$$r_{\Lambda_n}+\left\{\frac{\partial r_\Lambda}{\partial\boldsymbol{\sigma}'}\right\}_{n+1}\delta\Delta\boldsymbol{\sigma}'_{\boldsymbol{n+1}}+\left\{\frac{\partial r_\Lambda}{\partial\Delta\Lambda}\right\}_{n+1}\Delta t\delta\dot{\Lambda}_{n+1}=0 \tag{24}$$

The above equation can be rewritten for iteration procedure as follows:

$$-\left\{\frac{\partial r_\Lambda}{\partial\boldsymbol{\sigma}'}\right\}_{n+1}\boldsymbol{D}_{n+1}\delta\Delta\boldsymbol{\varepsilon}^e_{n+1}-\left\{\frac{\partial r_\Lambda}{\partial\Delta\Lambda}\right\}_{n+1}\Delta t\delta\dot{\Lambda}_{n+1}$$
$$=(\Lambda_{\boldsymbol{n+1}}-\Lambda_{\boldsymbol{n}})-\Delta t\dot{\Lambda}_{n+1} \tag{25}$$

By combining Eqs. (23) and (25), the system of nonlinear equations can be written in a matrix form as follows

$$\begin{bmatrix}\boldsymbol{I}+\Delta t\dot{\Lambda}_n\left\{\frac{\partial^2 p'_{eq}}{\partial\boldsymbol{\sigma}'^2}\right\}_{n+1}\boldsymbol{D}_{n+1} & \left\{\frac{\partial p'_{eq}}{\partial\boldsymbol{\sigma}'}\right\}_n\\ -\left\{\frac{\partial r_\Lambda}{\partial\boldsymbol{\sigma}'}\right\}_{n+1}\boldsymbol{D}_{n+1} & -\left\{\frac{\partial r_\Lambda}{\partial\Delta\Lambda}\right\}_{n+1}\end{bmatrix}\begin{Bmatrix}\delta\Delta\boldsymbol{\varepsilon}^e_{n+1}\\ \Delta t\delta\dot{\Lambda}_{n+1}\end{Bmatrix}$$
$$=\begin{Bmatrix}\Delta\boldsymbol{\varepsilon}^{trial}-\Delta\boldsymbol{\varepsilon}^e_n-\Delta t\dot{\Lambda}_n\left\{\frac{\partial p'_{eq}}{\partial\boldsymbol{\sigma}'}\right\}_n\\ (\Lambda_{\boldsymbol{n+1}}-\Lambda_{\boldsymbol{n}})-\Delta t\dot{\Lambda}_{n+1}\end{Bmatrix} \tag{26}$$

where $\boldsymbol{I}$ is the 6×6 identity matrix. Based on the above system of equations, the changes of elastic strain increment and the visco-plastic multiplier can be calculated using Newton–Raphson iteration. The iterative process can be considered complete when changes are very small.

The first iteration can start from the following system of equations

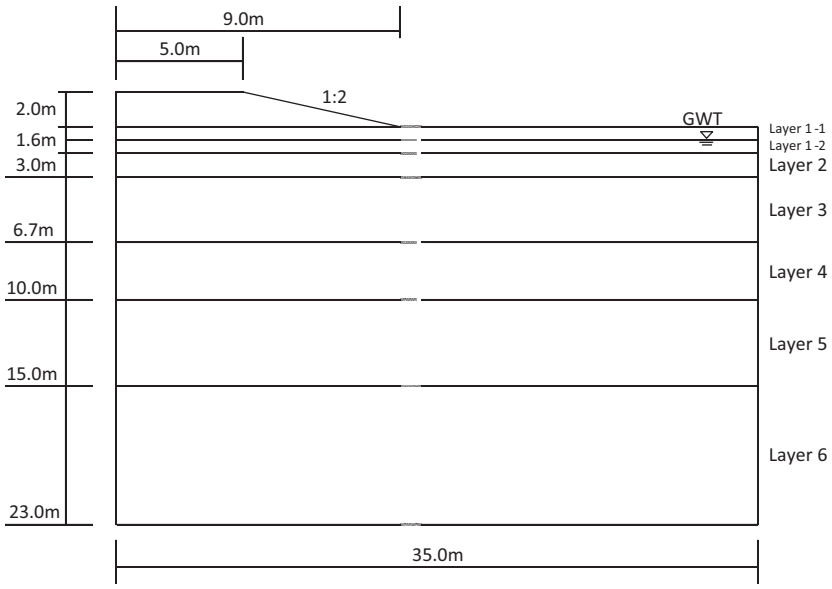

Fig. 5. Geometry of Murro test embankment.

Table 2
Parameters for constructed embankment.

E (kN/m^2)	ν'	φ' (°)	ψ' (°)	c' (kN/m^2)	γ (kN/m^2)
40,000	0.35	40	0	2	21

$$\begin{bmatrix} \boldsymbol{I} & \left\{\frac{\partial p'_{eq}}{\partial \boldsymbol{\sigma}'}\right\}_1 \\ -\left\{\frac{\partial r_A}{\partial \boldsymbol{\sigma}'}\right\}_1 \boldsymbol{D}_1 & -\left\{\frac{\partial r_A}{\partial \Delta A}\right\}_1 \end{bmatrix} \begin{Bmatrix} \delta\Delta\varepsilon_1^e \\ \Delta t\delta\dot{\Lambda}_1 \end{Bmatrix} = \begin{Bmatrix} 0 \\ 0 \end{Bmatrix} \tag{27}$$

The state variables are updated in each iteration. The resulting implementation is very robust, and furthermore, as demonstrated below, the model is able to represent single element simulation and the deformation-time response of Murro test embankment.

5. Numerical simulation: Creep-SCLAY1 versus ACM

This section discusses the predictive capability of Creep-SCLAY1 in comparison to the ACM model in a single element simulation to represent the isotach behaviour of normally consolidated natural clay. Parameters used for these simulations corresponding to Bothkennar clay are summarised in Table 1. Several publications (e.g. [31–35]) have shown the influence of step changes in the strain-rate on the stress–strain behaviour of soft soils. Important feature of isotach behaviour is that the effects of change in rate are continuous and the soil stays on the same stress–strain curve until the strain rate is changed. Immediately after an increase in strain rate, the stress–strain path is seen to jump upwards and show initially stiff response. If the strain rate is reduced back to the original strain rate, a downwards stress jump is observed, after which the path rejoins the original curve defined by the lower strain rate. The paths in stress–strain curves are indicated to be uniquely defined by the strain rate and the effects of strain rate changes are observed to be persistent, which is a characteristic of isotach behaviour, i.e., there is a unique stress–strain strain-rate relation for a given soil [34].

Fig. 4 shows a stepwise change in strain rate in undrained compression simulations using Creep-SCLAY1 and ACM for normally consolidated samples. Fig. 4 clearly demonstrates that ACM cannot simulate the isotach behaviour observed in natural soft clays under a stepwise change in strain rate due to the assumption of constant volumetric creep strain rates. Furthermore, experimental results e.g. by [24] demonstrate that with high shearing rates under undrained conditions it is possible the stress path to go well above the critical state line. ACM cannot reproduce that type of experimental behaviour due to the assumption on the constant viscoplastic volumetric strain rate.

Table 3
The initial values for state parameters of Murro clay.

Layer	Depth (m)	POP (kN/m^2)	e_0	α_0	In-situ K_0
1–1	0.0–0.8	20	1.4	0.63	1.25
1–2	0.8–1.6	10	1.4	0.63	1.25
2	1.6–3.0	2	1.8	0.63	0.34
3	3.0–6.7	2	2.4	0.63	0.35
4	6.7–10.0	2	2.1	0.63	0.40
5	10.0–15.0	2	1.8	0.63	0.42
6	15.0–23.0	2	1.5	0.63	0.43

5.1. Murro test embankment

The Murro test embankment was constructed on a 23 m deep deposit of medium sensitive clay near the town of Seinäjoki in Western Finland. The embankment has been monitored for a long time, since it was built in 1993, and it has been subjected to several studies (see e.g. [36–39]) due to decent instrumentation and extensive non-standard laboratory testing (for details see [4]). The latter, combined with long period of monitoring, does not apply to many case studies. Furthermore, it is the cases like Murro that are almost normally consolidated that are most difficult to model creep-wise, as creep strains get easily highly overpredicted. The almost normally consolidated clay is overlain by a 1.6 m thick overconsolidated dry crust and the underlying thick clay layer is almost normally consolidated and relatively homogeneous. The groundwater table is estimated to be at 0.8 m below ground level. Murro clay is highly strain anisotropic and time-dependent [4,39]. The Murro test embankment is 2 m high and 30 m long with a gradient of 1:2. The width of the top of the embankment is 10 m. The embankment material consists of crushed rock (biotite gneiss) with a grain size of 0–65 mm [38]. Construction of the embankment was completed in two days.

Table 4
Murro embankment parameters.

Layer	γ (kN/m^3)	ν'	M_c	M_e	k_x (m/day)	k_y (m/day)	ω	ω_d	λ^*	k^*
1–1	15.8	0.35	1.6	1.04	2.13E−04	1.64E−04	45	1.02	0.0667	4.20E−03
1–2	15.8	0.35	1.6	1.04	2.13E−04	1.64E−04	45	1.02	0.0667	4.20E−03
2	15.5	0.35	1.6	1.04	2.13E−04	1.64E−04	25	1.02	0.1786	1.07E−02
3	14.9	0.10	1.6	1.04	1.78E−04	1.34E−04	20	1.02	0.1471	1.06E−02
4	15.1	0.15	1.6	1.04	1.10E−04	9.07E−05	25	1.02	0.1161	9.07E−03
5	15.5	0.15	1.6	1.04	6.85E−05	5.48E−05	25	1.02	0.1143	1.21E−02
6	15.9	0.15	1.6	1.04	1.04E−04	8.22E−05	30	1.02	0.0560	1.60E−03

Table 5
Murro embankment parameters.

Layer	μ^*	τ day
1–1	8.69E−04	1
1–2	8.69E−04	1
2	2.33E−03	1
3	1.92E−03	1
4	1.52E−03	1
5	1.49E−03	1
6	7.30E−04	1

5.2. Finite element analysis

The construction and consolidation of Murro test embankment has been modelled with a plane strain finite element analysis using PLAXIS 2D Version 2012. Due to the symmetry of the problem, only half of the embankment was considered in the analyses. Fig. 5 shows the geometry and soil layers of Murro test embankment. The problem was simulated as large strain analysis using updated mesh and pore water option in PLAXIS. The finite element model was discretized by using a mesh consisting of 1416 15-noded triangular elements following mesh sensitivity studies. In the model the symmetry axis and the lateral boundary at a distance of 36 m were fixed in the horizontal direction and the bottom boundary at a depth of −23 m was fixed in both horizontal and vertical direction. The construction of the embankment was simulated as an undrained calculation phase followed by a fully coupled consolidation analysis.

The granular embankment fill was modelled with the simple linear elastic perfectly plastic Mohr Coulomb model and parameters are shown in Table 2. Parametric studies confirmed that the simulations are not sensitive to the embankment fill parameters, as the response is controlled by the underlying soft soil [38]. Karstunen et al. [38] divided the clay deposit into 7 layers based on available test data. Required parameters for Creep-SCLAY1 model were obtained from Karstunen et al. [39] and are summarised in Tables 3–5. For numerical stability pre-overburden pressure of 2 kPa has been assumed in the apparently normally consolidated layers.

Fig. 6 shows the measured vertical settlements at centre-line, and 2 m and 5 m off the centre-line, underneath the embankment, together with the Creep-SCLAY1 and ACM model predictions. Very good agreement is achieved between the measured and predicted settlements with Creep-SCLAY1. In contrast, the ACM model overpredicts the vertical settlement versus time compared to Creep-SCLAY1.

Fig. 7 presents the measured and predicted surface settlement immediately after the construction and during subsequent consolidation. Again, the Creep-SCLAY1 model captures well the surface settlements during the consolidation compared to the measurements. However, the model overestimates the settlement immediately after the construction which could be related to the fact that often the first measurements do not necessarily correspond to time zero. Though ACM predicts similar magnitudes in the beginning, with time the overprediction increases. Both models predict some creep deformation due to in situ stresses alone at the non-loaded section next to the lateral boundary.

Fig. 8 presents the comparison between the predicted and measured horizontal displacements, underneath the crest of the embankment and underneath the toe of the embankment, by the

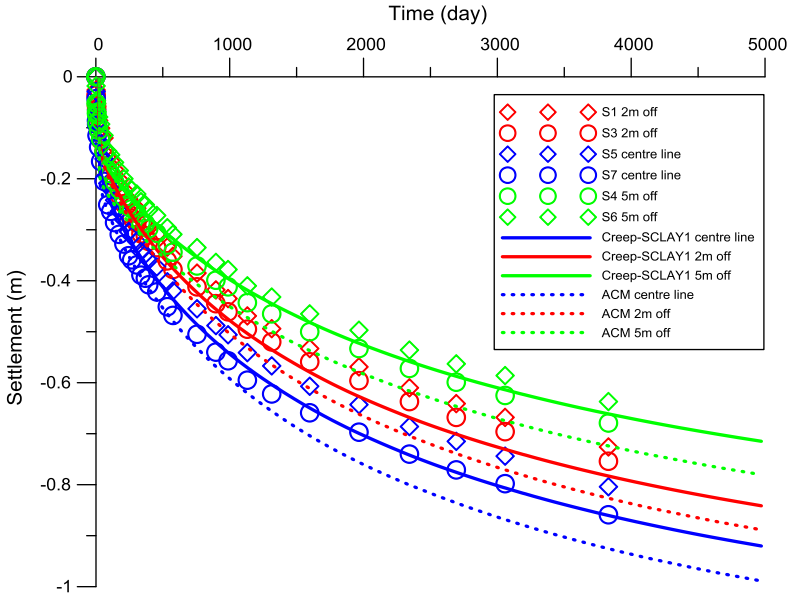

Fig. 6. Murro test embankment. Comparison between measured and predicted time-settlements (symbols and thick lines are measurement and predictions respectively).

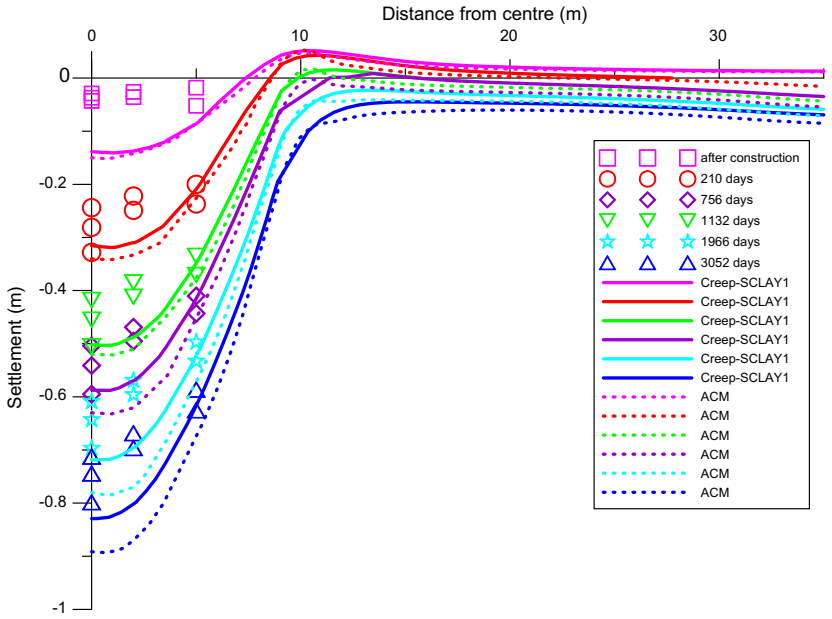

Fig. 7. Murro test embankment. Comparison between measured and predicted surface settlements (symbols and thick lines are measurement and predictions respectively).

Creep-SCLAY1 and ACM model. Very good agreement is achieved between the measured and predicted results for both cases with Creep-SCLAY1, although for the early stage of consolidation the horizontal displacements were overestimated. However, ACM significantly overpredicts the horizontal displacement, and even the predicted trend under the toe is not correct. This is due to the assumption of constant volumetric creep strain rates which results in shear strains being significantly overestimated.

For comparison, the influence of evolution of anisotropy in Creep-SCLAY1 is further studied by switching off the rotational hardening law (i.e. $\omega = 0$). This results in an anisotropic model with a fixed Normal Consolidation Surface. As shown in Fig. 9, when the evolution of anisotropy is ignored, the Creep-SCLAY1 model overestimates the settlements compared to the field measurements. The reason for this overprediction is that the model predicts lower soil stiffnesses when the evolution of anisotropy is ignored. When anisotropy evolves, energy is dissipated due to rotation of fabric, and therefore smaller settlements are predicted than with fixed anisotropy.

Even though the rate-dependency in the Creep-SCLAY1 model can be reduced by reducing the input value for the modified creep index, it is not possible to totally "switch off" the strain-rate effects. With a zero value of creep index, the model is undefined, as power β in Eq. (6) becomes undetermined. Decreasing creep index to very low values is also numerically challenging because of the power law. Hence, it is not possible to "switch off" the rate effects. Consequently, to study if it really is important to include rate-dependency in this particular problem, the embankment is also simulated using the equivalent (rate-independent) elasto-plastic S-CLAY1 [21] model. As shown in Fig. 10, the S-CLAY1 model significantly underpredicts the settlements with time. The results also demonstrate that it is important to account for strain rates even at the undrained construction stage, and as the time goes on, creep becomes increasingly significant. The results show that the time-dependent Creep-SCLAY1 model has clear advantages compared to the time-independent S-CLAY1 model in this respect.

6. Conclusions

This paper described a simple constitutive approach for modelling the creep behaviour of anisotropic clay that overcomes the problems associated with many of the rate-dependent models published so far. The foundation of the Creep-SCLAY1 model is the S-CLAY1 model [21], which has been extended to account for rate effects using ideas from Leoni et al. [3] and Grimstad et al. [20]. The model has been implemented as a user-defined soil model, using a fully implicit integration scheme with automatic substepping, resulting in a robust finite element formulation.

Unlike in classic Perzyna type overstress models, there is no purely elastic range in the Creep-SCLAY1 model. This makes the determination of the input parameters related to rate-dependency straightforward, as these can be derived directly from experimental data, without calibration of the values using test simulations. The existence of small positive volumetric creep rates upon unloading will also reduce the amount of heave in unloading problems, but as yet there is no systematic experimental data available to validate this feature of the model. A comprehensive validation programme on element level, including both loading and unloading loops, will take several years to complete and samples need to be tested within days from sampling in order not to affect the creep properties by disturbance by loss of suction and stress relaxation.

The advantage of using the adopted anisotropic formulation is that, unlike in the MCC model, the K_0 prediction of the model in the normally consolidated region is realistic, as long as the value for parameter ω_d is defined as proposed in Eq. (21). Furthermore, by using the concept of constant viscoplastic multiplier proposed by Grimstad et al. [20], it is possible to model the experimentally evidenced isotach behaviour. The model will also predict a unique critical state, regardless of the strain rate and stress path, as the normal compression surface rotates as a function of irrecoverable shear strains.

Given the model has a hierarchical structure, it is possible to switch off the evolution of anisotropy. When this is done, the predictions will generally be on the conservative side, i.e. vertical deformations will be over-predicted for embankment-type loading problems. Even though the rate-dependency in the Creep-SCLAY1 model can be reduced by reducing the input value for the modified creep index, it is not possible to totally "switch off" the strain-rate effects. If comparisons with equivalent rate-independent models are needed, simulations with the S-CLAY1 model should be performed, as was done for Murro test embankment.

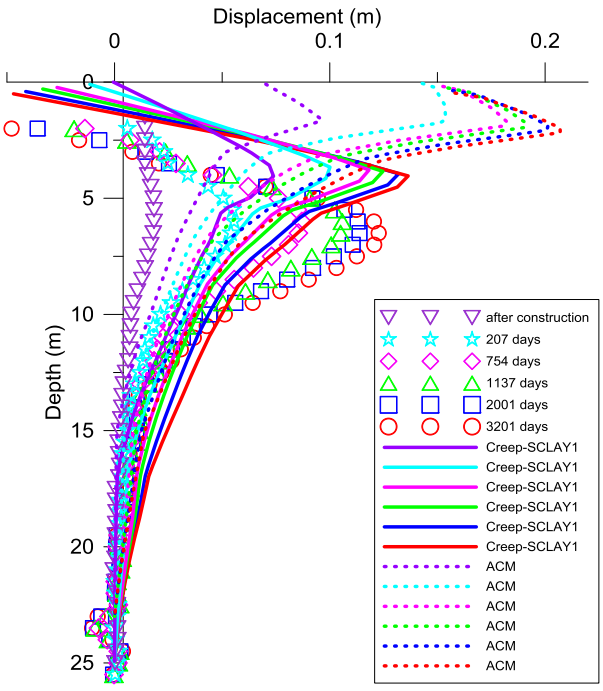

(a) Under crest

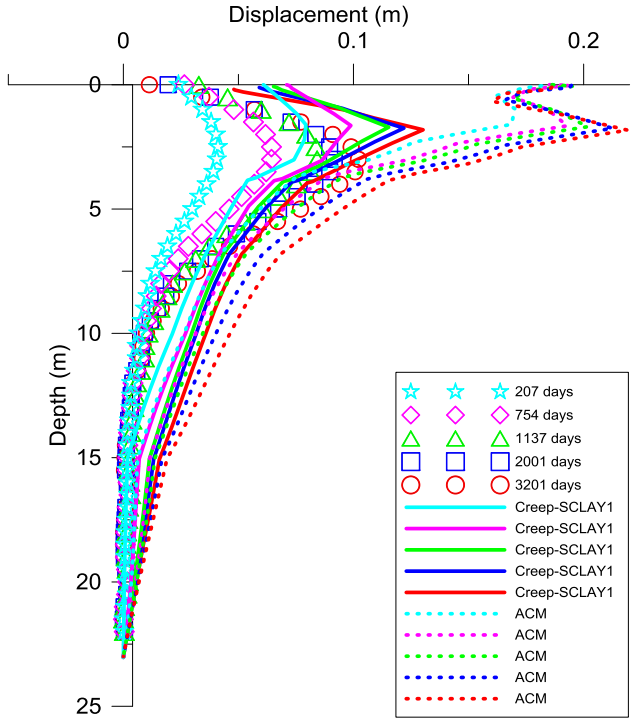

(b) Under toe

Fig. 8. Murro test embankment. Comparison between measured and predicted horizontal displacements (symbols and thick lines are measurement and predictions respectively).

Simulations on single element level, as well as boundary value level (the stress–strain–strain rate behaviour of the Murro test embankment) demonstrate that the Creep-SCLAY1 model gives realistic predictions. When compared with field deformations, in contrast to the predictions by ACM and an equivalent rate-independent model (S-CLAY1), the proposed model has a very good match with the measured data, both qualitatively and quantitatively. Simulations demonstrate that in the case of Murro test embankment, the rate-effects are significant already just after the construction stage, so it is not just a long-term effect where rate-dependent model is needed. Furthermore, the test embankment was also simulated with the model with fixed anisotropy. Results suggest that it is necessary to account for evolution of anisotropy in this problem, as with fixed anisotropy the deformations are over-predicted.

Due to the robustness of the implementation, the model is an ideal basis for further extensions, such as inclusion of effects of bonding and destructuration, as necessary for modelling the stress–strain response of highly sensitive clays.

Acknowledgements

The research was carried out as part of GEOINSTALL (Modelling Installation Effects in Geotechnical Engineering, PIAP-GA-2009-230638) and CREEP (Creep of Geomaterials, PIAP-GA-2011-286397) projects supported by the European Community through the programme Marie Curie Industry-Academia Partnerships and Pathways (IAPP) under the 7th Framework Programme. The support for the second author from BIG (Better Interaction in Geotechnics) project from the Swedish Transport Administration is also gratefully acknowledged. The authors would like to acknowledge the valuable suggestions and insights offered by Dr. Jelke Dijkstra at Chalmers University of Technology, Sweden.

Appendix A

Deviatoric stress tensor

$$\boldsymbol{\sigma}'_d = \begin{bmatrix} \sigma'_x - p' \\ \sigma'_y - p' \\ \sigma'_z - p' \\ \sqrt{2}\sigma'_{xy} \\ \sqrt{2}\sigma'_{yz} \\ \sqrt{2}\sigma'_{zx} \end{bmatrix} \tag{A.1}$$

Incremental deviatoric strain tensor

$$d\boldsymbol{\varepsilon}_d = \begin{bmatrix} \frac{1}{3}(2d\varepsilon_x - d\varepsilon_y - d\varepsilon_z) \\ \frac{1}{3}(-d\varepsilon_x + 2d\varepsilon_y - d\varepsilon_z) \\ \frac{1}{3}(-d\varepsilon_x - d\varepsilon_y + 2d\varepsilon_z) \\ \sqrt{2}d\varepsilon_{xy} \\ \sqrt{2}d\varepsilon_{yz} \\ \sqrt{2}d\varepsilon_{zx} \end{bmatrix} \tag{A.2}$$

Deviatoric fabric tensor

$$\boldsymbol{\alpha}_d = \begin{bmatrix} \frac{1}{3}(2\alpha_x - \alpha_y - \alpha_z) \\ \frac{1}{3}(-\alpha_x + 2\alpha_y - \alpha_z) \\ \frac{1}{3}(-\alpha_x - \alpha_y + 2\alpha_z) \\ \sqrt{2}\alpha_{xy} \\ \sqrt{2}\alpha_{yz} \\ \sqrt{2}\alpha_{zx} \end{bmatrix} = \begin{bmatrix} \alpha_x - 1 \\ \alpha_y - 1 \\ \alpha_z - 1 \\ \sqrt{2}\alpha_{xy} \\ \sqrt{2}\alpha_{yz} \\ \sqrt{2}\alpha_{zx} \end{bmatrix} \tag{A.3}$$

where components of fabric tensor have the property

$$\frac{1}{3}(\alpha_x + \alpha_y + \alpha_z) = 1 \tag{A.4}$$

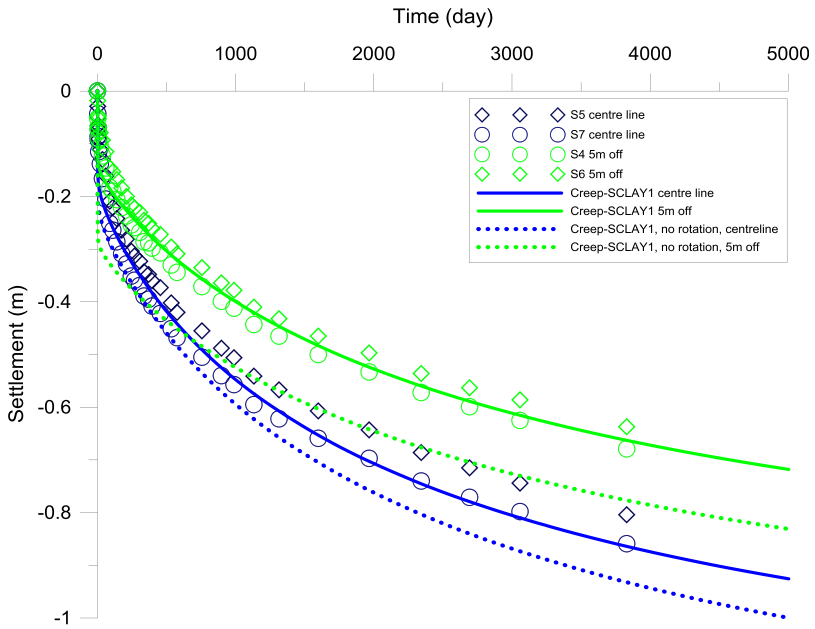

Fig. 9. Murro test embankment. Comparison between measured and predicted time-settlements with and without evolution of anisotropy (symbols and thick lines are measurement and predictions respectively).

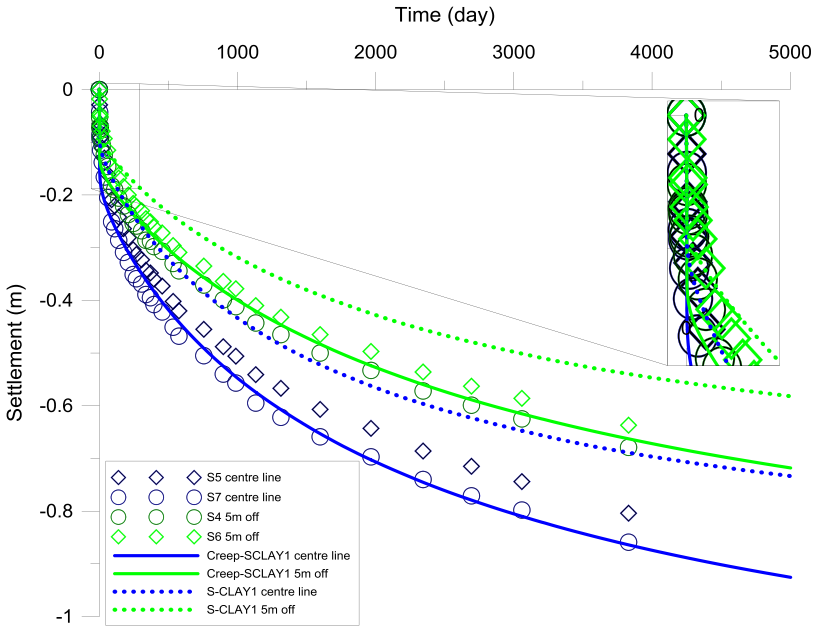

Fig. 10. Murro test embankment. Comparison between measured and predicted time-settlements with and without rate-dependency (symbols and thick lines are measurement and predictions respectively).

Scalar value of fabric tensor, α, which defines the orientation of the ellipses in triaxial stress space, can be defined as

$$\alpha^2 = \frac{3}{2}\boldsymbol{\alpha}_d : \boldsymbol{\alpha}_d \tag{A.5}$$

The initial components of α values is determined using the initial scalar value α_0

$$\left.\begin{aligned} \alpha_x &= \alpha_z = 1 - \tfrac{\alpha_0}{3} \\ \alpha_y &= 1 + \tfrac{2\alpha_0}{3} \\ \alpha_{xy} &= \alpha_{yz} = \alpha_{zx} = 0 \end{aligned}\right\} \tag{A.6}$$

The triaxial formulation of the Creep-SCLAY1 model is easily extended to three-dimensional stress space. The boldface characters are used to denote tensor quantities and subscript d denotes the deviatoric component. As the current stress surface (CSS) is similar to the elasto-plastic model S-CLAY1 [21], it can be expressed as:

$$p'_{eq} = p' + \frac{3}{2p'}\frac{\left(\boldsymbol{\sigma}'_d - \boldsymbol{\alpha}_d p'\right) : \left(\boldsymbol{\sigma}'_d - \boldsymbol{\alpha}_d p'\right)}{\left(M^2 - \frac{3}{2}\boldsymbol{\alpha}_d : \boldsymbol{\alpha}_d\right)} \tag{A.7}$$

The rotational hardening law describing the change of the orientation of the yield surface with irrecoverable straining can be expressed in general stress space as:

$$d\boldsymbol{\alpha}_d = \omega\left(\left[\frac{3\boldsymbol{\sigma}'_d}{4p'} - \boldsymbol{\alpha}_d\right]\langle d\varepsilon^c_v\rangle + \omega_d\left[\frac{\boldsymbol{\sigma}'_d}{3p'} - \boldsymbol{\alpha}_d\right]|d\varepsilon^c_d|\right) \tag{A.8}$$

The direction of creep strain rate is defined (associated flow rule) as

$$\dot{\boldsymbol{\varepsilon}}^c_{ij} = \dot{\Lambda}\frac{\partial p'_{eq}}{\partial \boldsymbol{\sigma}'_{ij}} \tag{A.9}$$

The total strain rate is sum of the elastic and creep part as

$$\dot{\boldsymbol{\varepsilon}}_{ij} = \dot{\boldsymbol{\varepsilon}}^e_{ij} + \dot{\boldsymbol{\varepsilon}}^c_{ij} \tag{A.10}$$

The elastic part of the strains modelled using Hooke's law

$$\dot{\boldsymbol{\sigma}}^e_{ij} = D_{ijhk}\dot{\boldsymbol{\varepsilon}}^e_{hk} \tag{A.11}$$

where the elastic stiffness matrix D_{ijhk} is

$$\boldsymbol{D}_{ijhk} = \frac{2G\upsilon'}{1-2\upsilon'}\boldsymbol{\delta}_{ij}\boldsymbol{\delta}_{hk} + G\left(\boldsymbol{\delta}_{ik}\boldsymbol{\delta}_{jh} + \boldsymbol{\delta}_{ih}\boldsymbol{\delta}_{jk}\right) \tag{A.12}$$

The second $(J_2)_\alpha$ and third $(J_3)_\alpha$ invariants of the modified stress deviator $\boldsymbol{\sigma}'_d - \boldsymbol{\alpha}_d p'$ are defined as:

$$(J_2)_\alpha = \frac{1}{2}\left[\left(\sigma'_x - p' - \alpha_{d,x}p'\right)^2 + \left(\sigma'_y - p' - \alpha_{d,y}p'\right)^2 + \left(\sigma'_z - p' - \alpha_{d,z}p'\right)^2 + \left(\sigma'_{xy} - \alpha_{d,xy}p'\right)^2 + \left(\sigma'_{yz} - \alpha_{d,yz}p'\right)^2 + \left(\sigma'_{zx} - \alpha_{d,zx}p'\right)^2\right] \tag{A.13}$$

$$\begin{aligned}(J_3)_\alpha = {} & \left(\sigma'_x - p' - \alpha_{d,x}p'\right)\left(\sigma'_y - p' - \alpha_{d,y}p'\right)\left(\sigma'_z - p' - \alpha_{d,z}p'\right) \\ & - \left(\sigma'_x - p' - \alpha_{d,x}p'\right)\left(\sigma'_{yz} - \alpha_{d,yz}p'\right)^2 \\ & - \left(\sigma'_y - p' - \alpha_{d,y}p'\right)\left(\sigma'_{zx} - \alpha_{d,zx}p'\right)^2 \\ & - \left(\sigma'_z - p' - \alpha_{d,z}p'\right)\left(\sigma'_{xy} - \alpha_{d,xy}p'\right)^2 \\ & - 2\left(\sigma'_{xy} - \alpha_{d,xy}p'\right)\left(\sigma'_{yz} - \alpha_{d,yz}p'\right)\left(\sigma'_{zx} - \alpha_{d,zx}p'\right)\end{aligned} \tag{A.14}$$

References

[1] Hinchberger SD, Rowe RK. Evaluation of the predictive ability of two elastic-viscoplastic constitutive model. Can Geotech J 2005;42(6):1675–94.
[2] Zhou C, Yin J-H, Zhu J-G, Cheng C-M. Elastic anisotropic viscoplastic modeling of the strain-rate dependent stress–strain behaviour of K0-consolidated natural marine clays in triaxial shear test. Int J Geomech 2006;5(3):218–32.
[3] Leoni M, Karstunen M, Vermeer PA. Anisotropic creep model for soft soils. Géotechnique 2008;58(3):215–26.
[4] Karstunen M, Yin Z-Y. Modelling time-dependent behaviour of Murro test embankment. Géotechnique 2010;60(10):735–49.
[5] Yin Z-Y, Karstunen M, Chang CS, Koskinen M, Lojander M. Modelling time-dependent behaviour of soft sensitive clay. J Geotech Geoenviron Eng 2011;137(11):1103–13.
[6] Perzyna P. The constitutive equations for rate sensitive plastic materials. Quart Appl Math 1963;20:321–32.
[7] Perzyna P. Fundamental problems in viscoplasticity. Adv Appl Mech 1966;9(3):244–377.
[8] Rowe RK, Hinchberger SD. The significance of rate effects in modelling the Sackville test embankment. Can Geotech J 1998;35(3):500–16.
[9] Adachi T, Oka F, Mimura M. An elasto–viscoplastic theory for clay failure. In: Proceedings of the 8th Asian regional conference on soil mechanics and foundation engineering, vol. 1. Kyoto, JSSMFE; 1987. p. 5–8.
[10] Sekiguchi H, Ohta H. Induced anisotropy and time dependency in clays. In: 9th ICSMFE, Tokyo, constitutive equations of Soils, vol. 17; 1977. p. 229–38.
[11] Nova R. A viscoplastic constitutive model for normally consolidated clay. In: Proceedings of the IUTAM symposium on deformation and failure of granular materials, vol. 1. Delft; 1982. p. 287–95.
[12] Liingaard M, Augustesen A, Lade PV. Characterization of models for time-dependent behavior of soils. Int J Geomech 2004;4(2):157–77.
[13] Yin J-H, Zhu JG, Graham J. Viscous-elastic-plastic modelling of one-dimensional time-dependent behaviour of clays. Can Geotech J 1988;26:199–209.
[14] Yin J-H, Graham J. Viscous-elastic–plastic modelling of one-dimensional time-dependent behaviour of clays. Can Geotech J 1989;26:199–209.
[15] Yin J-H, Graham J. Elastic viscoplastic modelling of time-dependent stress–strain behavior of soils. Can Geotech J 1999;36:736–45.
[16] Yin J-H, Zhu JG, Graham J. A new viscoplastic model for time-dependent behaviour of normally and overconsolidated clays: theory and verification. Can Geotech J 2002;39:157–73.
[17] Bodas Freitas TM, Potts DM, Zdravkovic L. A time dependent constitutive model for soils with isotach viscosity. Comp Geotech 2011;38(6):809–20.
[18] Vermeer PA, Stolle DFE, Bonnier PG. From the classical theory of secondary compression to modern creep analysis. In: Yuan, editor. Computer methods and advances in geomechanics. Rotterdam: Balkema; 1998.
[19] Vermeer PA, Neher HP. A soft soil model that accounts for creep. In: Proceedings of the international symposium on 'Beyond 2000 in Computational Geotechnics'. Amsterdam; 1999. p. 249–61.
[20] Grimstad G, Degado SA, Nordal S, Karstunen M. Modelling creep and rate effects in structured anisotropic soft clays. Acta Geotech 2010;5:69–81.
[21] Wheeler SJ, Näätänen A, Karstunen M, Lojander M. An anisotropic elasto-plastic model for soft clays. Can Geotech J 2003;40(2):403–18.
[22] Sivasithamparam N, Karstunen M, Brinkgreve RBJ, Bonnier PG. Comparison of two anisotropic creep models at element level. In: Hicks et al., editors. International conference on installation effects in geotechnical engineering. London: Taylor & Francis Group; 2013. p. 72–8.
[23] Karstunen M, Sivasithamparam N, Brinkgreve RBJ, Bonnier PG. Modelling rate-dependent behaviour of structured clays. In: Hicks et al., editors. International conference on installation effects in geotechnical engineering. London: Taylor & Francis Group; 2013. p. 43–50.
[24] Yin JH, Chang CM. Comparison of strain-rate dependent stress–strain behaviour from K0-consolidated compression and extension tests on natural Hong Kong Marine deposits. Marine Georesour Geotechnol 2006;24(2):119–47.
[25] Karstunen M, Koskinen M. Plastic anisotropy of soft reconstituted clays. Can Geotech J 2008;45(3):314–28.
[26] Matsuoka H, Nakai T. Stress-deformation and strength characteristics of soil under three different principal stresses. Proc Jap Soc Civ Eng 1974;232:59–70.
[27] Sheng D, Sloan S, Yu H. Aspects of finite element implementation of critical state models. Comput Mech 2000;26:185–96.
[28] Roscoe KH, Burland JB. On the generalised stress–strain behaviour of 'wet' clay. J Eng Plast 1968:553–609.
[29] Zentar R, Karstunen M, Wiltafafsky C, Schweiger HF, Koskinen M. Comparison of two approaches for modelling anisotropy of soft clays. In: Pande, Pietruszczak, editors. Proceedings of the 8th international symposium on numerical models in geomechanics (NUMOG VIII). Rome; 2002. p. 115–21.
[30] de Borst R, Heeres O. A unified approach to the implicit integration of standard, non-standard and viscous plasticity models. Int J Numer Anal Meth Geomech 2002;26:1059–70.
[31] Vaid Y, Campanella R. Time-dependent behaviour of undisturbed clay. ASCE J Geotech Eng Div 1977;103(7):693–709.
[32] Tavenas F, Leroueil S, La Rochelle P, Roy M. Creep behaviour of an undisturbed lightly overconsolidated clay. Can Geotech J 1978;15(3):402–23.
[33] Graham J, Crooks J, Bell A. Time effects on the stress–strain behaviour of natural soft clays. Géotechnique 1983;33(3):327–40.
[34] Leroueil S, Marques M. State of art: importance of strain rate and temperature effects in geotechnical engineering. measuring and modelling time dependent behaviour of soils. ASCE, Geotech Spec Public 1996;61:1–60.
[35] Tatsuoka F, Ishihara M, Di Benedetto H, Kuwano R. Time-dependent shear deformation characteristics of geomaterials and their simulation. Soils Found 2002;42(2):103–38.
[36] Koskinen M, Lojander M, Tolla P, Vepsäläinen P. Numerical analysis on Murro test embankment. In: Mestat, editor. Proceedings of the numerical methods in geotechnical engineering (NUMGE). Paris, France; 2002. p. 397–402.
[37] Karstunen M, Koskinen M. Anisotropy and destructuration of Murro clay. In: Proceedings of the advances in geotechnical engineering skempton conference, vol. 1. London (UK); 2004. p. 476–87.
[38] Karstunen M, Krenn H, Wheeler SJ, Koskinen M, Zentar R. The effect of anisotropy and destructuration on the behaviour of Murro test embankment. Int J Geomech 2005;5(2):87–97. ASCE.
[39] Karstunen M, Rezania M, Sivasithamparam N, Yin Z-Y. Comparison of anisotropic rate-dependent models for modelling consolidation of soft clays. Int J Geomech 2012. http://dx.doi.org/10.1061/(ASCE)GM.1943-5622.0000267, ISSN 1532-3641.